Microporous and Mesoporous Materials 185 (2014) 113–120

Contents lists available at ScienceDirect

Microporous and Mesoporous Materials

journal homepage: www.elsevier.com/locate/micromeso

Preparation of Cu–mordenite by ionic exchange reaction under milling: A favorable route to form the mono-(μ-oxo) dicopper active species

Arianee Sainz-Vidal [a], Jorge Balmaseda [b], Luis Lartundo-Rojas [c], Edilso Reguera [a,*]

[a] Centro de Investigación en Ciencia Aplicada y Tecnología Avanzada, Unidad Legaria, Instituto Politécnico Nacional, México D.F., Mexico
[b] Departamento de Polímeros, Instituto de Investigaciones en Materiales, Universidad Nacional Autónoma de México, México D.F., C.P. 04510, Mexico
[c] Centro de Nanociencias y Micro-Nanotecnologías, Instituto Politécnico Nacional, México, D.F., Mexico

ARTICLE INFO

Article history:
Received 30 August 2013
Received in revised form 16 October 2013
Accepted 4 November 2013
Available online 13 November 2013

Keywords:
Zeolite
Ionic exchange
Copper μ-oxo dimer
Solid state reaction
Adsorption

ABSTRACT

Cu-exchanged mordenite samples were prepared using both solid state and aqueous solution ionic reactions. The obtained materials were then characterised from UV–vis, XPS, and TPR data in order to obtain information on the state of copper in the exchanged samples. Three types of copper species were identified, surface clusters of Cu_2O, hydrated Cu(II) ions with two slightly different coordination environments, and mono (μ-oxo) dicopper core, $[Cu_2O]^{2+}$, located in β type channels for samples activated on heating in the presence of oxygen. The formation of this last species, active for the methane conversion into methanol, was found to be particularly favored for the solid state ionic exchange reaction, and it is detected as an intense charge transfer band at 400 nm in the recorded UV–vis spectra and a well-defined peak at 936.34 eV of binding energy in the XPS spectra. The stabilisation of this dicopper core is the main distinctive difference between the exchange reactions in the solid state and in solution. The appearance of this bridged binuclear Cu^{2+} species was also detected in the recorded TPR profiles. According to the recorded CO_2 adsorption isotherms, the ionic exchange process modifies the accessible pore volume but the material preserves its porous features. The ability of that core for the low temperature methane conversion into methanol was confirmed recording chromatographic profile at different temperatures.

1. Introduction

Zeolites, both natural and synthetic, related to their porous open framework, large surface area and ionic exchange properties, have found industrial applications in heterogeneous catalysis, separation and drying processes, water softening, environmental remediation, etc. [1]. The ionic exchange process is probably the most widely used route to modify the zeolites properties and it is commonly carried out from aqueous solution of the ion to be introduced as charge-balancing species [2,3]. This process is also possible in gas phase [4–8] and solid state [8–16]. The gas phase ion exchange is based on a reaction at high temperature between the zeolite and a gaseous source of the cation to be exchanged. Moreover, the solid state method is performed milling the mixture of the involved zeolite and the salt used as the ion source. The Cu–mordenite samples studied in this work were prepared from Na–mordenite and copper (II) acetate using that last ionic exchange route. The ionic exchange under milling facilitates the cation entrance to the zeolite framework because the hydration effect on the effective ion size is minimised, enabling its diffusion through the material porous framework [17]. The naked Cu(II) ion has an ionic radius between 0.71 and 0.87 Å, depending on their coordination [18]. However, in its hydrated form the effective ionic radius is estimated to be in the 4–5 Å range [19]. In addition, ionic exchange process in solid state takes place away from the equilibrium conditions; on the microcrystals colliding the liberated energy leads to the appearance of hot points where local phase transitions, occurrence of redox reactions, and formation of solid solution and metastable phases are possible [20]. Furthermore, the particles fracture under milling induces the solid activation through the appearance of structural defects and active sites. However, all these features for the ionic exchange in solid state and their effects on the state of the incorporated ion remain poorly documented. This contribution attempts to shed light on such possible effects for the case of Cu-exchanged mordenite.

Mordenite crystallises with an orthorhombic unit cell in the *Cmcm* space group with cell parameters $a = 18.13$, $b = 20.5$, $c = 7.52$ Å [21]. Its porous framework is formed by parallel 12-membered (aperture 7×6.5 Å) and 8-membered (aperture 5.7×2.6 Å) rings channels which remain communicated by a less compressed 8-membered rings channel (aperture 3.4×4.8 Å) [22]. In this framework there are three sites for the charge balancing cation, two of them located in the interconnecting channels and the third one in the large 12-membered rings channel [23]. The aperture of the large channel is enough to allow the ionic exchange

* Corresponding author. Tel./fax: +52 55 53954147.
E-mail address: edilso.reguera@gmail.com (E. Reguera).

1387-1811/$ - see front matter © 2013 Elsevier Inc. All rights reserved.
http://dx.doi.org/10.1016/j.micromeso.2013.11.009

and the entrance of small molecules, up to 6.5 Å of size, to interact with the channel surface and with extra framework species.

Copper exchanged zeolites have received large attention in the last decades for their catalytic activity for both nitrogen oxides (NO_x) decomposition [9] and low temperature methane conversion into methanol [24–26]. NO_x emission is one of the main contaminants from the exhaust gas of diesel engines [27]. This specie is involved in the ground-level ozone formation, acid rain, and it contributes to the greenhouse effect [28]. Cu–mordenite is an exchanged zeolite with high performance for nitrogen oxides decomposition [29]. On the material heating in the presence of NO_x the copper atom subtracts the oxygen atom from the nitrogen oxide and a feature band at 400 nm is observed in the corresponding UV–vis spectrum [30]. The same band at about 400 nm appears when the Cu exchanged zeolite, particularly ZSM-5 and mordenite, are heated in the presence of oxygen, but not when the heat treatment is carried out in an atmosphere free of O_2 or NO_x [31].

The low temperature catalytic conversion of methane into methanol is an attractive option instead the technology of high temperature methane reforming for methanol production [32]. The technology of hydraulic fracturing for shale natural gas extraction has increased the worldwide availability of methane as the main constituent of natural gas and from this fact, the interest in obtaining methanol from methane through a low cost process. Methanol is a liquid fuel at room temperature facilitating its use in automotive and stationary technologies and as raw material for the chemical industry. That possibility would be available using oxygen activated Cu exchange zeolites related to the formation of the copper species with the characteristic 400 nm absorption band [24,26]. Such property of Cu-exchanged zeolites is ascribed to the formation of mono (μ-oxo) dicopper core, $[Cu_2O]^{2+}$ [33,34]. The CuOCu angle of about 140° favors the interaction of the oxygen atom with the guest methane molecule within the porous framework and the subtraction of a proton from the molecule [35]. To the best of our knowledge, the effect of the exchange route on the formation of that active copper species has not been studied.

The above mentioned properties of Cu-exchanged zeolites and the solid state ionic exchange route to favor the formation of the copper μ-oxo dimer are the main motivations of this study. The Cu-exchanged mordenite samples under study were characterised from X-ray diffraction (XRD), thermogravimetric (TG), IR spectroscopy, CO_2 adsorption, and chemical analyses data. The state of copper in the exchanged mordenite samples was evaluated from UV–vis spectroscopy, X-ray photoelectron spectroscopy (XPS), and hydrogen temperature-programmed reduction (TPR) data. The ability of oxygen activated Cu-exchanged mordenite samples for the methane conversion into methanol was explored from chromatographic profiles. For comparison, samples of Cu–mordenite prepared under ionic exchange in aqueous solution were also studied. From the obtained data, the effect of the ionic exchange route on the state of copper is discussed.

2. Experimental

Na-mordenite (CVB 10 A, Si/Al = 13) from Zeolyst International was used for the ionic exchange with copper (II) acetate 98% (Sigma–Aldrich) as the metal source, for both solid state and aqueous solution exchange reactions. For the solid state exchange reaction a weight proportion of 1:0.7 of zeolite to copper acetate was used. The mixture was milled in a planetary ball mill for 1 h (sample labeled as CuMorSS1) and by hand using an agate mortar for 6 h (sample labeled as CuMorSS2), both at room temperature. The samples CuMorSS1 and CuMorSS2 were then stabilised under dried nitrogen flow for 24 h at 27 °C, washed several times with distilled water to remove the excess of copper acetate and of the formed sodium acetate and finally submitted to heating in air for 5 h at 600 °C in order to decompose the salt fraction that remains impregnated in the solid. The exchange in aqueous solution was performed under stirring at 45 °C during 24 h, then separating the solid fraction by centrifugation and repeating two additional exchange reactions under similar conditions. The obtained exchange zeolite sample was washed several times with distilled water until to obtain a filtrate free of acetate ion, according to IR spectroscopy of the dried fraction. The separated solid was finally heated for 5 h in air at 600 °C in order to decompose the remaining salt. This third sample is labeled as CuMorSol. For the Cu-exchanged samples, previous to the heat treatment at 600 °C, the labels CuMorSS1R, CuMorSS2R, CuMorSolR will be used. The resulting exchanged Cu–modernite samples were characterised from chemical analyses, XRD, TG, IR, UV–vis, TPR, XPS and adsorption data.

XRD powder patterns were recorded with $CuK_{\alpha 1}$ radiation in a D8 Advance diffractometer from Bruker. The lattice parameters were obtained by the Le Bail pattern fitting method. IR spectra were run using both Nujol mulls and KBr pressed disks with a Spectrum One spectrophotometer from Perkin Elmer. UV–vis spectra were collected in diffused reflectance mode with a Perkin-Elmer spectrometer equipped with an integration sphere. The TG curves were recorded in air and under a nitrogen flow of 100 mL/min in a modulated high resolution thermobalance (Q 5000 from TA Instruments), using the high resolution dynamic method with a heating rate of 3 °C min^{-1}. The TPR experiments were carried out using Auto Chem 2910 equipment (from Micromeritics) and a quartz reactor under a flow of 10% H_2/Ar (50 mL min^{-1}) and the sample heating from room temperature up to 973 K at a heating rate of 10 K min^{-1}. The hydrogen consumption in the reduction reaction was monitored with a thermoconductivity detector. The recorded profiles were then fitted using Gaussian peak-shape in order to estimate the H_2 consumption involved in the observed processes (see Supplementary Information). XPS spectra were collected using a K-Alpha spectrometer from Thermo Scientific with monochromatic AlKα (1486 eV) radiation and an energy resolution of 0.5 eV. The recorded spectra were fitted through a combination of Gaussian peaks using the software provided with the spectrometer. The CO_2 adsorption isotherms were recorded at 273 K in the pressure range of 10^{-6}–760 Torr using an ASAP 2020 analyzer from Micromeritics. Carbon dioxide, related to its geometry, is an appropriate adsorbate to explore the porous structure of materials containing narrow channels. The experimental adsorption isotherms were fitted with Langmuir–Freundlich type isotherm equation derived from vacancy solution theory, $n_a = \frac{n_m (p_{eq}/p_{1/2})^{1/g}}{1+(p_{eq}/p_{1/2})^{1/g}}$, where, n_a is the quantity adsorbed, p_{eq} is the equilibrium pressure, n_m is the limit adsorption capacity of the zeolite, $p_{1/2}$ is the pressure at which $n_a = n_m/2$ and g is a constant related with relative activity coefficient f by $f = (1 - n_a/n_m)^{g-1}$ [36]. The non-linear fitting of Langmuir–Freundlich equation to experimental data was performed with the Microsoft Excel 2010 Solver. The standard deviations of: n_m, $p_{1/2}$ and g were estimated with the Solver Statistics macro provided on the CD-ROM that accompanies Ref. [37]. The chemical potential of adsorbate μ_a, relative to liquid chemical potential at isotherm temperature $\mu(T, p_v)$, was calculated by equation $\mu_a(T, p_{eq}) = \mu_l(T, p_v) + R\ln\{(p_{1/2}/p_v)[n_a/(n_m - n_a)]^g\}$. In order to corroborate the low temperature methane oxidation selectivity of the Cu-exchanged mordenite samples, stainless steel columns of 2.2 mm diameter and 30 cm in length were packed with 300 mg of Cu-exchanged zeolite samples and installed in an HP 5890 Series II chromatograph with FID detector. The methane elution peaks were recorded at column temperatures of: 50, 80, 90, 100, 150, 200 and 250 °C. The chromatographic profile was recorded at

different consecutive 0.04 μl methane injections for a given temperature in the column in order to follow the stability of the active species.

3. Results and discussion

3.1. Characterisation of the samples under study

The zeolite framework is preserved on the ionic exchange reactions and then after the heat treatment. The initial, exchanged and calcined samples have similar XRD patterns, except a minor volume contraction for unit cell (Table 1 and Supplementary Information). The TG curves and IR spectra are also in favor of the material stability on the mentioned treatment (Supplementary Information). IR spectra for the parent Na–mordenite and the exchanged samples are practically identical. The TG curves reveal a smaller hydration degree for the exchanged samples obtained through the solid state reaction. It seems, for the samples obtained by the exchange route free of solvent a smaller free volume is available to accommodate water molecules. This could be attributed to a higher exchange degree for that exchange route. The recorded carbon dioxide adsorption isotherms are characteristic of porous solids but for the exchanged and calcined samples a reduction for the accessible volume of 16% is observed (Fig. 1, and Table 2). Such accessible volume reduction could be ascribed to a greater space occupied by the copper species loaded in the porous framework, in concordance with the evidence obtained from the TG curves. Besides, after the copper exchange, the absolute value of the chemical potential with respect to liquid adsorbate decreases (Fig. 1, Inset), suggesting the presence of a copper species with weak interaction with carbon dioxide or the reduction of the accessibility of the adsorbate to the adsorption domain. In Table 1 the exchange degree, unit cell parameters, IR absorption bands and the number of water molecules calculated from the TG curves for the original Na–mordenite and the exchanged samples are summarised. The higher copper loaded amount is observed for the samples obtained under milling. It seems the smaller effective ionic radius for copper (II) ion in absence of solvent favors its intracrystalline diffusion and the access to practically all the possible positions for the charge-balancing cation. This result is in accordance with the CO_2 adsorption data and TG curves where a smaller accessible volume was observed for the samples obtained by the solid state ionic exchange reactions.

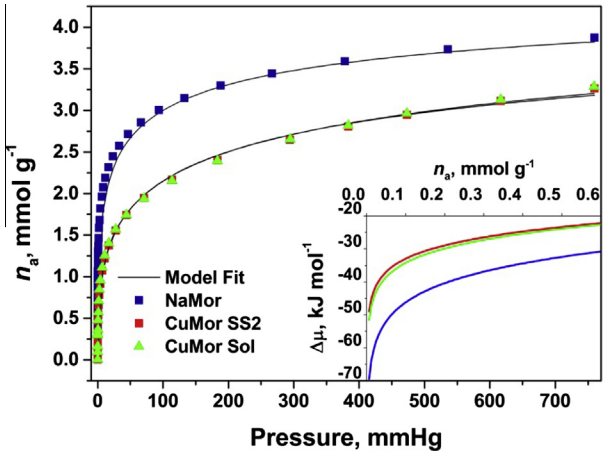

Fig. 1. Carbon dioxide adsorption isotherms at 0 °C for mordenite samples, and the chemical potential with respect to liquid adsorbate as a function of the quantity adsorbed (Inset).

Table 2
Binding energy for Cu 2p3/2 XPS peak for Cu species in Cu–mordenite samples.

Sample	Compound	Cu2p3/2 eV	Atomic (%)
CuMorSS1	Cu(I) oxide	932.1	10
	Cu(II) oxide	933.8	58
	Cu(II) hydroxide	935.1	9
	Cu(II) mono (μ-oxo)	936.3	23
CuMorSS2	Cu(I) oxide	932.1	2
	Cu(II) oxide	933.8	51
	Cu(II) hydroxide	935.1	14
	Cu(II) mono (μ-oxo)	936.3	33
CuMorSS2R	Cu(I) oxide	932.1	14
	Cu(II) oxide	933.8	60
	Cu(II) hydroxide	935.1	26
CuMorSol	Cu(I) oxide	932.1	7
	Cu(II) oxide	933.8	69
	Cu(II) hydroxide	935.1	15
	Cu(II) mono (μ-oxo)	936.3	18
CuMorSolR	Cu(I) oxide	932.1	15
	Cu(II) oxide	933.8	60
	Cu(II) hydroxide	935.1	25

Table 1
Chemical and structural characterisation of the Cu-exchanged mordenite samples under study.

Data			Samples				
			CuMor SS1	CuMor SS2	CuMorSS2R	CuMor Sol	CuMorSolR
Exchange degree (%)			58	76	61	73	56
Unit cell parameters	*a*, Å		18.117 (1)	18.0988 (8)	18.1369 (5)	18.1077 (7)	18.1444 (9)
	b, Å		20.403 (2)	20.3722 (7)	20.4048 (4)	20.3822 (6)	20.4022 (8)
	c, Å		7.512 (2)	7.5017 (2)	7.5060 (1)	7.5065 (2)	7.5054 (3)
IR bands (cm^{-1})	OH (ν)	HF	3663	3640	3632	3663	3633
		LF	3440	–	3450	3440	3443
	O–H–O (δ)		1633	1633	1633	1633	1633
	T–O (ν_{as})	Ext.	1227	1227	1222	1227	1222
		Int.	1077	1077	1066	1077	1066
	T–O (ν_s)	Ext.	808	808	808	808	808
		Int.	725	738	738	745	720
	Single 4-MR		634	634	626	634	626
	Double ring		580	580	580	580	580
			560	560	560	560	560
	T–O (δ)		464	464	461	464	461
H_2O molecules/unit cell			21	20	24	25	26

ν, OH stretching vibration; HF, high frequency; LF, LF; δ, O-H-O bending; ν_s, T–O symmetric and asymmetric stretching (ν_{as}); 4-MR, single 4-membered ring; δ, T–O bending.

3.2. UV–vis spectra of Cu-exchanged mordenite

UV–vis spectra were recorded in order to shed light on the oxidation state and coordination number for the exchanged copper atoms and on the nature of their ligands. Copper (II) complexes have characteristic absorption bands in the visible region related to d–d transitions. The energetic separation of t_{2g} and e_g orbitals depends on both, the metal coordination number and ligands nature. From this fact the frequency where these bands are observed provides information on the metal coordination environment. For Cu(I) no information is obtained from the UV–vis spectra because it has a $3d^{10}$ electronic configuration. The reduction to Cu(0) and the metal clusters formation is detected in the spectra as appearance of a plasmon resonance absorption band. In this case the incident electromagnetic radiation is absorbed through excitation of collective oscillations of the metal particle electron cloud.

Fig. 2 shows the UV–vis spectra for the series of Cu-exchanged mordenite samples. For comparison, the spectrum of the parent Na–mordenite was included. The broad absorption band observed near 800 nm was ascribed to pseudo-octahedral Cu(II) with water molecules as ligands without discard the presence of oxygen atoms from the zeolite framework as metal ligands. The Jahn–Teller effect in Cu(II) octahedral complexes leads to the coordination environment distortion with the appearance of two possible d–d transitions in the visible region. These bands occur very close together and are observed as an asymmetric broad band. For a pseudo-octahedral coordination environment where the Jahn–Teller distortion is not possible, also two d–d transitions are observed. This explains the spectral features observed for the band around 800 nm. For the samples submitted to heat treatment (CuMorSol, CuMorSS1, CuMorSS2), the maximum of that band is observed at 779, 771 and 767 nm, respectively. Such blue shift relatively to the Cu-exchanged samples before the heat treatment (CuMorSolR, CuMorSS1R, CuMorSS2R), whose maximum is found at 800 nm, corresponds to an increase in the ligand field related to the replacement of water molecules by framework oxygen atoms from Al tetrahedra.

The absorption band observed with the maximum at 400 nm was interpreted as a charge transfer $O_{bridge} \rightarrow Cu$ transition by formation of mono (μ-oxo) dicopper core, $[Cu_2O]^{2+}$ (Fig. 2) on the sample heating in air. This band is absent in the spectra of Na–mordenite and in the Cu-exchanged samples before the heat treatment, indicating that the dimer is formed on the sample heating in the presence of oxygen. The formation of this dimer has been reported for Cu–mordenite and Cu-ZSM-5 when these materials are heated in the 280–700 °C temperature range under an atmosphere containing O_2 and/or NO_2 [35]. Within the herein considered series of Cu-exchanged mordenite, the band at 400 nm is particularly intense for the samples prepared by the solid state exchange reaction. Such behavior was interpreted as related to a higher degree of exchange for this exchange route and to the relatively small size for the copper (II) in absence of solvent which facilitates its accessibility to the β channel in the zeolite framework (Fig. 3). According to the mordenite channels topology and distance between Al atoms [33], the dicopper core is probably formed in the β channel from the copper occupying two neighboring extra-framework positions for the exchanged metal, similar to the reported configuration for the dicopper species formed in ZSM-5 Cu exchanged zeolite [35]. The location of charge balancing metal ions in exchanged zeolites is controlled by both the Si/Al ratio and the distribution of Al atoms in the framework [33]. The framework negative charge to be compensated with the exchangeable cation is mainly located in the environment of Al atoms. In this sense, the most probable framework ligands for the exchanged metal are oxygen atoms from Al tetrahedra.

The presence of mono (μ-oxo) dicopper cores is in agreement with the decrease of absolute value of the chemical potential with respect to liquid adsorbate, observed in the adsorption experiments after Cu exchange (Fig. 1, Inset). The large dimensions of the cores force the CO_2 molecules to be further away from the charge centers. These steric restrictions weaken the short-range interactions between CO_2 quadrupole moments and cores field gradient.

In the long-wavelength region the spectrum for the parent mordenite and all the exchanged samples two absorption maxima at the same position are observed (see Supplementary Information). The first maximum is found at 1412 nm with a shoulder at 1470 nm and it corresponds to the combination vibration band (2ν) of water molecule [38–40]. The second maximum, observed at 1907 nm with a shoulder at 1974 nm was ascribed to the combination vibration band ($\nu + \delta$) also of water [38,39].

Fig. 4 shows the UV–vis spectra for CuMor samples reduced under a H_2 flow during the TPR experiments (discussed below). The adsorption bands around 800 and 440 nm, ascribed to Cu(II) and mono (μ-oxo) dimer, respectively, have disappeared and a broad band below 600 nm is now observed. That band is characteristic of plasmon resonance absorption related to the formation of small particles copper in metallic state [41]. These small copper particles may be formed from the reduction of copper oxide present on the surface at the end of the exchange process, and by migration of some copper atoms to the zeolite crystallites surface. The spectrum with the most pronounced maximum, at ~564 nm, corresponds to the sample of CuMorSS2, which has the highest amount of loaded copper from the ion exchange process in the solid state. The slight

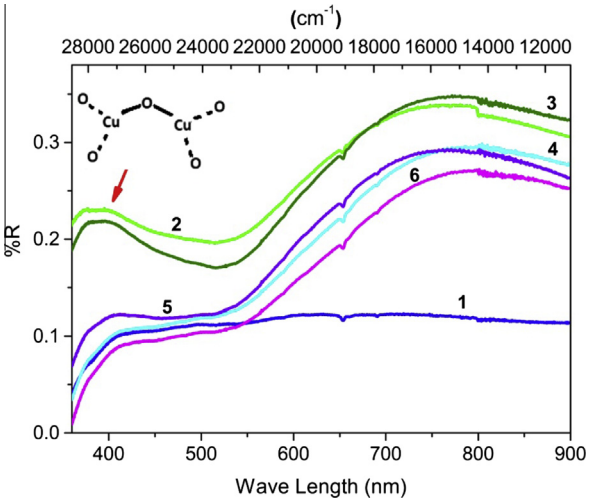

Fig. 2. UV–Vis DR spectra of: (1) parent NaMor, (2) CuMor SS1, (3) CuMor SS2, (4) CuMor SS2R, (5) CuMor Sol, and (6) CuMor SolR.

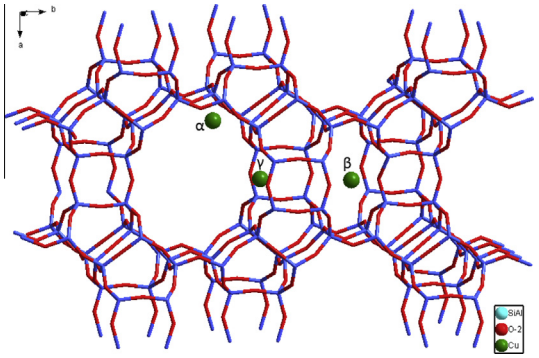

Fig. 3. Extra-framework cationic sites for dehydrated mordenite [23,64].

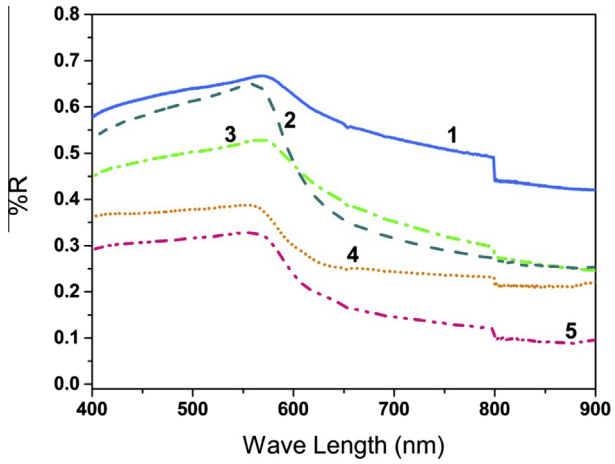

Fig. 4. UV–Vis absorption spectra of reduced CuMor samples: (1) CuMor Sol, (2) CuMor SS2, (3) CuMor SS1, (4) CuMor SS2R and (5) CuMor SolR.

red shift for the plasmon resonance peak observed for the samples CuMorSol and CuMorSS1, with the maximum at ~572 nm, was ascribed to an increase for the metal particle size [42].

3.3. XPS spectra of Cu-exchanged mordenite

X-ray photoelectron spectroscopy provides information on the electronic configuration, coordination number and nature of the ligands for the element involved in the photoelectron emission. Such information is obtained from the binding energy (BE) for the emitted photoelectron. In this study the recorded XPS spectra were used to shed light on the nature of the different copper species found in the exchanged mordenite samples before and after the heat treatment.

Fig. 5 shows the Cu_2p XPS spectra for the Cu-exchanged mordenite samples prepared by the two ion exchange routes. For the calcined samples (CuMorSS1, CuMorSS2 and CuMorSol) the photoemission profile can be fitted using up to four Gaussian peaks with binding energies (BE) of 932.1, 933.8, 935.1 and 936.3 eV. According to the available literature on XPS spectra for copper compounds, the three first values of BE correspond to Cu_2O, CuO and Cu $(OH)_2$ species [43]. The first peak at 932.1 eV was ascribed to Cu(I) species, produced by Cu(II) partial reduction during the high temperature treatment. The reduction upon zeolite activation in vacuum at elevated temperature is a known behavior for transition metals [44–49]. The second and third peaks, at 933.8 and 935.1 eV, respectively, were assigned to Cu(II) cations loaded in the channels of the zeolite framework with different coordination environments where water molecules and oxygen atoms from the framework are participating. According to UV–vis spectra, the fourth peak at 936.3 eV, only observed for the calcined samples (CuMorSS1, CuMorSS2 and CuMorSol), could be ascribed to the presence of mono (μ-oxo) dicopper (II) species where an extraframework oxygen atom participates. That fourth peak is only observed when in the UV–vis spectra the absorption at 400 nm ascribed to presence of mono (μ-oxo) dicopper (II) species is detected. No reference XPS spectra were found reported for this last copper core. For the sample obtained by ionic exchange in solution (CuMorSol) the peak corresponding to that active copper species is of relatively low intensity (Fig. 5), in correspondence with the low intensity for the $O_{bridge} \rightarrow Cu$ transition detected in the recorded UV–vis spectra (Fig. 2). From the relative peak area of the fitted XPS spectra, the amount of formed mono (μ-oxo) dicopper species in the samples under study follows the order CuMorSS2 (33%) > CuMorSS1 (23%) > CuMorSol (18%). Definitely, the formation of that binuclear copper species is favored for the solid state reaction. The XPS spectra for the exchanged samples without heat treatment (CuMorSS1R, CuMorSS2R and CuMorSolR) are free of the signal ascribed to the active mono (μ-oxo) dicopper species (Fig. 5). These spectra can be fitted with only the three Gaussian peaks assigned to Cu(I) and Cu(II) species with BE below 936 eV (Fig. 5 and Table 3). The Cu(I) cations in these samples may be originated in the Cu(II) partial reduction caused by the ultra-high vacuum of the XPS chamber and the X-ray radiation [50,51].

3.4. TPR profile for the Cu-exchanged mordenite

The temperature at which a metal species, loaded in zeolites, is reduced under a hydrogen (H_2) flow depends on both, its stability and the accessibility of hydrogen molecule to the structural sites where that species is found. The amount of reduced metal species

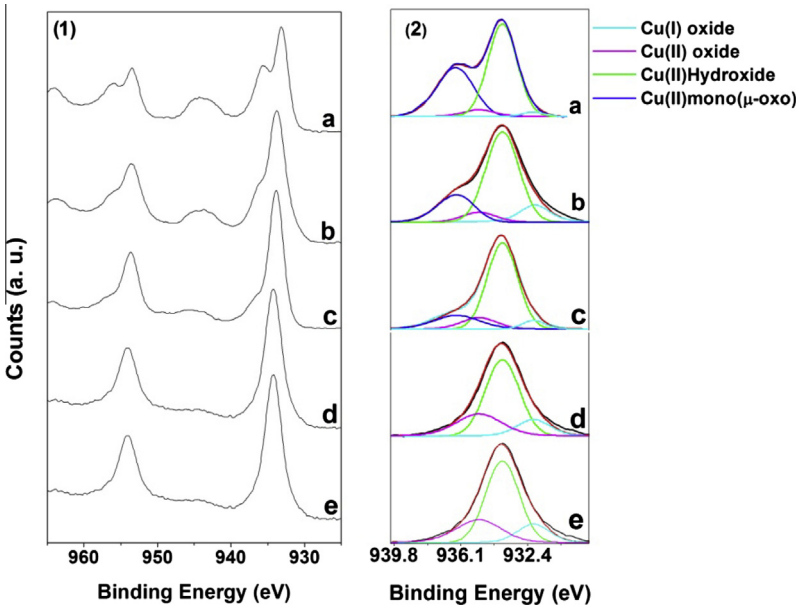

Fig. 5. XPS spectra for Cu–mordenite samples: (a) CuMorSS2, (b) CuMorSS1, (c) CuMorSol, (d) CuMorSS2R and (f) CuMorSolR. Only the Cu2p and Cu2p3/2 core levels region is shown.

Table 3
Parameters of Langmuir–Freundlich equation estimated by non-linear fitting of carbon dioxide adsorption isotherms.

Sample	n_p (mmol g^{-1})	g	$P_{0.5\ mm}$ (Hg)
NaMor	6.2 ± 0.9	3.6 ± 0.4	107.36 ± 0.02
CuMor SS2	5.1 ± 0.4	2.5 ± 0.1	249.18 ± 0.03
CuMor Sol	5.7 ± 0.6	2.7 ± 0.1	389.79 ± 0.03

can be estimated from the relative H_2 consumption in the reduction process. Fig. 6 shows the recorded TPR profile for all the herein considered Cu-exchanged mordenite samples. The thermogram fitting with Gaussian profiles is available from Supplementary Information. For the samples without heat treatment, three well defined peaks are observed. The narrow peak below 200 °C was ascribed to small clusters of Cu_2O and CuO species formed at the external zeolite particles surface. Under the same experimental conditions, for bulk CuO this reduction reaction is detected at 204 °C (Fig. 6, Inset). The observed shift toward low temperature of that reduction reaction for the zeolite samples is probably related to the small size for the cuprous and cupric clusters. This hypothesis is supported by the recorded XRD powder patterns where such clusters are not detected. XRD informs us on the presence of solid phases with long range crystallinity ordering and for particle size below 5 nm the fraction of surface atoms, which are out of their ideal Wickoff positions, is relatively large producing highly diffuse and weak diffraction signal [52]. The remaining two broader peaks observed at about 220 and 300 °C were interpreted as related to the reduction of Cu(II) species to Cu(0) in two different structural sites. This assignment is based in the calculated H_2 consumption corresponding to these two reduction reactions. In analogous previous studies on Cu-exchanged zeolites using TPR data [53–62], the appearance of two well defined high temperature peaks in the reduction profile has been attributed to a two stage-reduction ($Cu^{2+} \rightarrow Cu^{+} \rightarrow Cu^{0}$) of a one type of Cu ion [53–59] or to a single-stage reduction ($Cu^{2+} \rightarrow Cu^{0}$) of two different types of Cu^{2+} ions [59–61]. The comparison of the ratio of consumed H_2/Cu for each maximum corresponds to the model of a single-step reduction process of

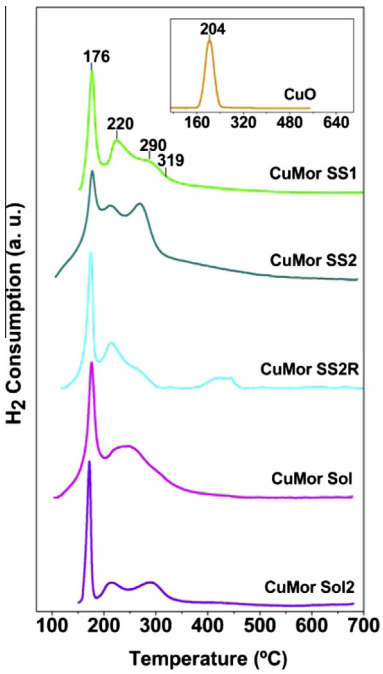

Fig. 6. TPR profiles of CuMor samples. The fitted curves using Gaussian profiles are available from Supplementary Information.

different types of Cu^{2+} species because the quantities are quite different and the total consumed H_2/Cu suggests that only a very little amount of the total copper remains unreduced (see Supplementary Information) . This is also supported by the reduction of bulk CuO where a single reduction reaction is observed (Fig. 6, Inset). An analogue single step reduction behavior is expected for the surface cuprous and cupric oxide clusters. Partially dehydrated mordenite has three possible structural positions (α, β, γ in Fig. 3) for exchangeable cations [10,45,46]. The observed reduction reactions at about 220 and 300 °C were assigned to Cu(II) ion in these three possible sites. The hydrogen uptake at 200 °C was ascribed to Cu(II) ion in the most accessible α sites in the largest channel, while for the less accessible sites (β and γ) the reduction reaction must be observed at higher temperature, in this case it is observed at 300 °C. When the H_2 consumption profiles are fitted with a superposition of Gaussian peaks the greatest peak-width is obtained for the reduction reaction at 300 °C (see Supplementary Information). The ratio of the peak, and total thermogram areas suggest that the high temperature peak could be related to the reduction reaction of Cu(II) in two sites of similar accessibility and with analogous coordination environments (β and γ sites).

In the TPR curves for the samples submitted to heat treatment three well-defined peaks plus a broad high temperature shoulder for the H_2 consumption related to reduction of copper species are observed (Fig. 6). The low temperature narrow peak at 176 °C was assigned to the already mentioned small clusters of Cu_2O and CuO. The peak at 220 °C is interpreted as the reduction of copper (II) ion in α sites while the peak assigned for the metal (Cu) in β and γ sites now appears splitted in a peak at 290 °C for γ sites and the high shoulder ascribed to copper (II) ions in β sites. This interpretation is consistent with the above-discussed UV–vis and XPS spectroscopic data. The high temperature shoulder only appears when in the UV–vis spectra the feature absorption band at 400 nm is detected and when in the XPS spectra the peak of highest binding energy, at 936.34 eV, is observed. As already-discussed, in mordenite the site β has the appropriate channel topology and the required Al–Al distance to support the formation of the mono (μ-oxo) dicopper core where the copper atoms are found linked to oxygen atoms from Al tetrahedral (Fig. 2) [33].

3.5. Methane oxidation to methanol in the Cu-exchanged mordenite

The mono (μ-oxo) dicopper core, $[Cu_2O]^{2+}$, formed during Cu-exchanged zeolites samples heated in air, is a well-established active site in the selective methane oxidation at low temperatures for ZSM-5 and mordenite type zeolites [26,49]. The performed chromatographic experiment in this work also confirms such behavior. Methane is an adsorbate usually used as reference to calculate the retention time in inverse gas chromatography studies related to separation of hydrocarbons mixtures because it is poorly retained (adsorbed) by materials. The methane adsorption forces are dominated by dispersive type interactions. By this fact, the observed peak area dependence on the column temperature (Fig. 7) was ascribed to the adsorbate oxidation. The formed species (methanol) is a polar molecule which could be strongly adsorbed in the zeolite polar framework and it is not detected in the chromatographic experiment. In reported studies on this subject, the methanol detection is carried out from ^{13}C NMR spectra of the adsorbed product after an extraction with a mixture of water and acetonitrile [24]. The Inset of Fig. 7 shows the methane peak area as a function of the column temperature. An increase in the temperature leads to a decrease of the eluted methane amount which is ascribed to its conversion into methanol. A pronounced decrease in the peak area is observed at 90 °C, with maximum activity at 150 °C (Fig. 7). This is in accordance with the reported behavior

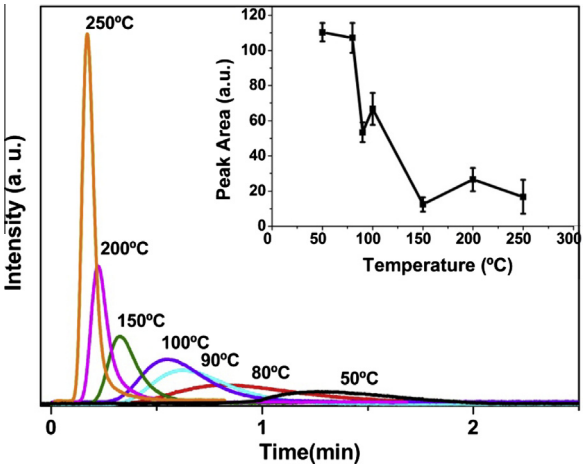

Fig. 7. Methane elution peaks at different column temperatures in a column filled with the CuMorSS2 sample. Inset: the peak area versus column temperature plot.

for that copper species for the methane oxidation to form methanol [63].

4. Conclusions

The copper ionic exchange in Na–mordenite samples was carried under milling and in aqueous solution for comparative purposes. The higher exchange degree was observed for the solid state route. The solid state reaction facilitates the metal ion diffusion through the porous framework and the accessibility to all available sites for the exchangeable charge-balancing cation in the material structure. All the experimental evidence indicates that the solid state method followed by a high temperature treatment under oxidative atmosphere is the most favorable route for the formation of mono (μ-oxo) dicopper core. When Cu-exchanged samples were heated in air at 600 °C in the recorded UV–vis spectra a feature absorption band at 400 nm was observed which has been ascribed to a charge transfer band $O_{bridge} \rightarrow Cu$ by formation of a mono (μ-oxo) dicopper core. This band is particularly intense for the samples prepared by milling. In the recorded XPS spectra this copper dimer is detected through also an intense peak at the highest binding energy (936.3 eV) within the observed copper species in this study. When TPR profiles for Cu-exchanged samples before and after the heat treatment at 600 °C are compared, the formation of the mono (μ-oxo) dicopper species is detected as appearance of a broad shoulder above 300 °C. The high temperature where that shoulder is observed suggests a relatively high stability for the copper atom when it is coordinated to two oxygen atoms from the Al tetrahedra and to the extralattice oxygen bridge between neighboring copper atoms. The material containing that mono (μ-oxo) dicopper species was tested for the methane conversion into methanol and the expected behavior was observed. To the best of our knowledge, this is the first report where a comparative study on the role of the exchange route on the formation of the active mono (μ-oxo) dicopper species is discussed.

Acknowledgements

The authors thank Dr. N. Barba, Dr. H. López, Dr. A. Lemus, M. A. Canseco and Lazaro Huerta for the invaluable experimental facility. A.S.-V. thanks CONACyT and IPN (Mexico) for PhD scholarship grants. This study was partially supported by the projects CONACyT-2009-01-129048, 2010-117373, 2011-174247, I010/296/2012, 2012-193850 and 2012-154626.

Appendix A. Supplementary data

Supplementary data associated with this article can be found, in the online version, at http://dx.doi.org/10.1016/j.micromeso.2013.11.009.

References

[1] S.M. Auerbach, K.A. Carrado, P.K. Dutta, Handbook of Zeolite Science and Technology, Marcel Dekker, New York, 2003.
[2] A.A. Zagorodni, Ion Exchangers, their Structure and Major Properties, in Ion Exchange Materials, Elsevier, Oxford, 2007 (Chapter 2) pp. 9–54.
[3] Y. Kuroda, A. Kotani, H. Maeda, H. Moriwaki, T. Morimato, M. Nagao, J. Chem. Soc. Faraday Trans. 88 (1992) 1583.
[4] C. Lamberti, S. Bordiga, M. Salvalaggio, G. Spoto, A. Zecchina, F. Geobaldo, G. Vlaic, M. Bellatreccia, J. Phys. Chem. B 101 (1997) 344.
[5] C. Lamberti, S. Bordiga, A. Zecchina, M. Salvalaggio, F. Geobaldo, C. Otero, J. Chem. Soc. Faraday Trans. 94 (1998) 1519.
[6] C. Prestipino, G. Berlier, F.X. Llabrés i Xamena, G. Spoto, S. Bordiga, A. Zecchina, G. Turnes Palomino, T. Yamamoto, C. Lamberti, Chem. Phys. Lett. 363 (2002) 389.
[7] V. Bolis, A. Barbaglia, S. Bordiga, C. Lamberti, A. Zecchina, J. Phys. Chem. B 108 (2004) 9970.
[8] S. Bordiga, E. Groppo, G. Agostini, J.A. van Bokhoven, C. Lamberti, Chem. Rev. 113 (2013) 1736.
[9] A.V. Kucherov, A.A. Slinkin, Zeolites 7 (1987) 43.
[10] Z. Li, K. Xie, R.C.T. Slade, Appl. Catal. A 209 (2001) 107.
[11] H.G. Karge, H.K. Beyer, Solid-State Ion Exchange in Microporous and Mesoporous Materials, Springer-Verlag, Berlin, 2002.
[12] Y. Kuroda, K. Yagi, N. Horiguchi, Y. Yoshikawa, R. Kumashiro, M. Nagao, Phys. Chem. Chem. Phys. 5 (2003) 3318.
[13] Y. Zhang, I.J. Drake, D.N. Briggs, A.T. Bell, J. Catal. 244 (2006) 219.
[14] Y. Zhang, I.J. Drake, A.T. Bell, Chem. Mater. 18 (2006) 2347.
[15] I.J. Drake, Y. Zhang, D. Briggs, B. Lim, T. Chau, A.T. Bell, J. Phys. Chem. B 110 (2006) 11654.
[16] I.J. Drake, Y. Zhang, M.K. Gilles, C.N. Teris Liu, P. Nachimuthu, R.C.C. Perera, H. Wakita, A.T. Bell, J. Phys. Chem. B 110 (2006) 11665.
[17] R.P. Townsend, E.N. Coker, Stud. Surf. Sci. Catal. 137 (2001) 467.
[18] R.D. Shannon, Acta Cryst. A 32 (1976) 751.
[19] H.Y. Chen, L. Chen, J. Lin, K.L. Tan, Inorg. Chem. 36 (1997) 1417.
[20] E.M. Gutman, Mechanochemistry of Materials, Cambridge International Science, London, 1998.
[21] T. Armbruster, M.E. Gunter, in: D.I. Bish, D.W. Ming (Eds.), Natural Zeolites: Occurrence, Properties, Applications Reviews, Mineralogy and Geochemistry: 45. Mineralogical Society of America and Geochemical Society, Washington, DC, 2001.
[22] M.H. Kim, I.S. Nam, Y.G. Kim, J. Catal. 179 (1998) 350.
[23] W.J. Mortier, Extraframework Cationic Positions in Zeolites, Elsevier, Amsterdam, 1982.
[24] M.H. Groothaert, P.J. Smeets, B.F. Sels, P.A. Jacobs, R.A. Schoonheydt, J. Am. Chem. Soc. 127 (2005) 1394.
[25] P. Vanelderen, R.G. Hadt, P.J. Smeets, E.I. Solomon, R.A. Schoonheydt, B.F. Sels, J. Catal. 284 (2011) 157.
[26] P. Vanelderen, J. Vancauwenbergh, B.F. Sels, R.A. Schoonheydt, Coord. Chem. Rev. 257 (2013) 483.
[27] J.B. Heywood, Internal Combustion Engine Fundamentals, MacGraw-Hill International, Singapore, 1988.
[28] United States Environmental Protection Agency, Human Health and Environmental Effects of Emissions from Power Generation, Washington, DC, 2013. <http://www.epa.gov/captrade/documents/power.pdf>.
[29] M.N. Moura de Olivera, C. Monteiro Silva, R. Moreno-Tost, T. López-Farias, A. Jiménes-López, E. Rodríguez Castellón, Appl. Catal. B 88 (2009) 420.
[30] M.H. Groothaert, K. Lievens, J.A. van Bokhoven, A.A. Battiston, B.M. Weckhuysen, K. Pierloot, R.A. Schoonheydt, Chem. Phys. Chem. 4 (2003) 626.
[31] M.H. Groothaert, J.A. van Bokhoven, A.A. Battiston, B.M. Weckhuysen, R.A. Schoonheydt, J. Am. Chem. Soc. 125 (2003) 7629.
[32] W.-H. Cheng, H.H. Kung, Methanol Production and Use, Marcel Dekker, New York, 1994.
[33] J. Dědeček, Z. Sobalík, B. Wichterlová, Sci. Eng. 54 (2012) 135.
[34] F. Giordanino, P.N.R. Vennestrom, L.F. Lundegaard, F.N. Stappen, S. Mossin, P. Beato, S. Bordiga, C. Lamberti, Dalton Trans. 42 (2013) 12741.
[35] J.S. Woertink, P.J. Smeets, M.H. Groothaert, M.A. Vance, B.F. Sels, R.A. Schoonheydt, E.I. Solomon, Proc. Natl. Acad. Sci. USA 106 (2009) 18908.
[36] T.S. Yakubov, B.P. Bering, M.M. Dubinin, V.V. Serpinskii, Izv. Akad. Nauk SSSR, Ser. Khim 2 (1977) 463.
[37] E.J. Billo, Excel® for Chemists, A Comprehensive Guide, John Wiley & Sons Inc., New Jersey, 2011.
[38] J. Dědeček, B. Wichterlová, J. Phys. Chem. B 103 (1999) 1462.
[39] G. Hersberg, Molecular Spectra and Molecular Structure II, Infrared and Raman Spectra of Polyatomic Molecules, New York, 1945.
[40] J.H. Shen, A.C. Zettlemoyer, K. Kller, J. Phys. Chem. 84 (1980) 1453.
[41] I. Lisiecki, M.P. Pileni, J. Phys. Chem. B 99 (1995) 5077.
[42] V. Petranovskii, V. Gurin, N. Bogdanchikova, A. Licea-Claverie, Y. Sugi, E. Stoyanov, Mater. Sci. Eng. A 332 (2002) 174.

[43] C.D. Wagner, A.V. Naumkin, A. Kraut-Vass, J.W. Allison, C.J. Powell, J.R. Rumble, NIST Standard Reference Database 20, Version 3.4 (web version), Washington, DC, 2003. <http://srdata.nist.gov/xps/>.
[44] M. Iwamoto, H. Yahiro, K. Tanda, N. Mizuno, Y. Mine, S. Kagawa, J. Phys. Chem. 95 (1991) 3727.
[45] S.C. Larsen, A. Aylor, A.T. Bell, J.A. Reimer, J. Phys. Chem. 98 (1994) 11533.
[46] Y. Kuroda, Y. Yoshikawa, S.-I. Konno, H. Hamano, H. Maeda, R. Kumashiro, M. Nagao, J. Phys. Chem. 99 (1995) 10621.
[47] V. Bolis, S. Maggiorini, L. Meda, F. D'Acapito, G.T. Palomino, S. Bordiga, C. Lamberti, J. Chem. Phys. 113 (2000) 9248.
[48] F.X. Llabrés i Xamena, P. Fisicaro, G. Berlier, A. Zecchina, G.T. Palomino, C. Prestipino, S. Bordiga, E. Giamello, C. Lamberti, J. Phys. Chem. B 107 (2003) 7036.
[49] P.J. Smeets, J.S. Woertink, B.F. Sels, E.I. Solomon, R.A. Schoonheydt, Inorg. Chem. 49 (2010) 3573.
[50] W. Grunert, N.W. Hayes, R.W. Joyner, E.S. Shpiro, M.R.H. Siddiqui, G.N. Baeva, J. Phys. Chem. 98 (1994) 10832.
[51] C. Dossi, A. Fusi, G. Moretti, S. Recchia, R. Psaro, Appl. Catal. A 188 (1999) 107.
[52] A. Gomez, J. Rodríguez-Hernández, E. Reguera, Powder Diffr. 21 (2007) 27.
[53] J.Y. Kim, J.A. Rodriguez, J.C. Hanson, A.I. Frenkel, P.L. Lee, J. Am. Chem. Soc. 125 (2003) 10684.
[54] M.M. Pavlyuchenko, Y.S. Rubinchik, J. Appl. USSR 24 (1951) 751.
[55] G. Fierro, M. Lojacomo, M. Inversi, P. Porta, R. Lavecchia, F. Cioci, J. Catal. 148 (1994) 709.
[56] J. Sárkány, W.M.H. Sachtler, Zeolites 14 (1994) 7.
[57] D.L. Hoang, T.T.H. Dang, J. Engeldinger, M. Schneider, J. Radnik, M. Richter, A. Martin, J. Solid State Chem. 184 (2011) 1915.
[58] C. Torre-Abreu, M.F. Ribeiro, C. Henrigues, D. Delahay, Appl. Catal. B Environ. 14 (1997) 261.
[59] S.J. Gentry, N.W. Shuwt, A. Jones, J. Chem. Soc. Faraday I 75 (1979) 1688.
[60] L. Martins, R.P. Sobradiel Peguin, E.A. Urquieta-González, Quim. Nova 29 (2006) 223.
[61] A. Jones, B. McNicol, Temperature-Programmed Reduction for Solid Materials Characterisation, Marcel Dekker, New York, 1986.
[62] M. Afzal, G. Yasmeen, M. Saleem, J. Afzal, J. Therm. Anal. Cal. 62 (2000) 721.
[63] P.J. Smeets, M.H. Groothaert, R.M. van Teeffelen, H. Leeman, E.J.M. Hensen, R.A. Schoonheydt, J. Catal. 245 (2007) 358.
[64] W.J. Mortier, J. Phys. Chem. 81 (1977) 1334.